JOURNAL OF SOLID STATE CHEMISTRY 116, 265–274 (1995)

Characterization by TEM of Local Crystalline Changes during Irradiation Damage of Hydroxyapatite Compounds

S. Nicolopoulos,* J. M. González-Calbet,†,‡ M. P. Alonso,* M. T. Gutierrez-Ríos,* M. I. de Frutos,* and M. Vallet-Regí*,‡,[1]

*Departamento de Química Inorgánica y Bioinorgánica, Facultad de Farmacia, Universidad Complutense, 28040 Madrid, Spain; †Departamento de Química Inorgánica, Facultad de Químicas, Universidad Complutense, 28040 Madrid, Spain; and ‡Instituto de Magnetismo Aplicado, RENFE-UCM, Apdo. 155, 28230 Las Rozas, Madrid, Spain

Received February 28, 1994; in revised form October 20, 1994; accepted October 20, 1994

Local crystalline changes during transmission electron microscopy (TEM) examination of hydroxyapatite (OHAp) compounds have been revealed by combining electron diffraction analysis and the Moiré fringe method. The latter is a sensitive tool for the detection of small crystal variations induced by beam irradiation damage in the OHAp structure. TEM observations suggest that a hexagonal ($P6_3/m$) to monoclinic (with $b = 2a$) transformation could occur as a possible result of beam-induced stoichiometry changes. Such order–disorder transformations seem to be related to very small local crystal lattice rotations as deduced by the changing of the Moiré patterns period under the electron beam. © 1995 Academic Press, Inc.

INTRODUCTION

Human calcified tissues (i.e., bones, teeth, and cartilage) are composed to a very large extent of hydroxyapatite (OHAp) crystals of chemical composition $Ca_{10}(PO_4)_6(OH)_2$ (1–3). Synthetic OHAp is a biomaterial that poses challenges for use in clinical applications (4–6). The physicochemical properties of this compound used as biomaterial depend strongly on crystal stoichiometry (i.e., Ca/P ratio) and also on the surface state (absorbed ions or molecules).

The chemical composition and original symmetry of the OHAp structure (Table 1) may be altered during TEM observations (7–12). It has been shown that by working at 200, 300, and 400 kV, electrons may displace or even eject many ions from their original sites (especially Ca ions), leading to the destruction of the OHAp structure and to the formation of either CaO or α-$Ca_3(PO_4)_3$ (α-TCP) structures (7, 13–16). The possible existence of the monoclinic $P2_1/b$ OHAp structure has also been discussed (19, 20), but the influence of the beam irradiation on the stability of this phase is not clear.

[1] To whom correspondence should be addressed.

Several irradiation-induced phenomena have been observed during the examination of OHAp crystals by TEM: orientation-dependent damage in the form of void formation or uniform destruction of the crystal structure, surface roughening, etc. (7).

In this paper, the damage phenomena in the OHAp structure induced by irradiation at 200 kV are studied. In contrast to previous HREM and diffraction studies dealing with irradiation damage in the OHAp structure, we have used the sensitive Moiré fringe method, which, coupled with microdiffraction and optical diffraction analysis, can reveal new aspects of local structure and symmetry of OHAp evolution with irradiation.

EXPERIMENTAL

Hydroxyapatite was prepared by the reaction of $Ca(NO_3)_2 \cdot 4H_2O$ (1 M) and KH_2PO_4 (0.6 M) in aqueous solution. OHAp powders were characterized by X-ray diffraction with Cu$K\alpha$ radiation on a Siemens D-5000 diffractometer.

Chemical analysis was performed by using the atomic absorption method for calcium (Perkin–Elmer 2280) and a spectrophotometric nitromolybdatevanadate method for phosphorus.

Infrared spectroscopic measurements have been carried out at room temperature using a Perkin–Elmer Model 283 instrument, with the samples being prepared as KBr pellets.

The OHAp sample for TEM was prepared by dry dispersion on a copper grid covered with a thin holey carbon film. The TEM study was performed on a JEOL 2000 FX electron microscope operated at 200 kV and equipped with a side-entry double-tilt specimen stage. Distances and angles of the Moiré pattern were measured directly on the photographs and on the optical diffractograms, as they present a calibration scale as well. Multislice calculations have been performed with the NCEMSS program

0022-4596/95 $6.00
Copyright © 1995 by Academic Press, Inc.
All rights of reproduction in any form reserved.

TABLE 1
Crystallographic Parameters of Hydroxyapatite (22)

Lattice	Hexagonal, $a = b = 0.9432$ nm, $c = 0.6881$ nm, and $Z = 2$
Space group	$P63/m$ (No. 176)
Atomic coordinates	O(1) in 6(h): 0.3272, 0.4837, 0.25, occ[a] = 1
	O(2) in 6(h): 0.5899, 0.4666, 0.25, occ = 1
	O(3) in 12(i): 0.3457, 0.2595, 0.0736, occ = 1
	P in 6(h): 0.3999, 0.3698, 0.25, occ = 1
	Ca(1) in 4(f): 1/3, 2/3, 0.0010, occ = 1
	Ca(2) in 6(h): 0.2464, 0.9938, 0.25, occ = 1
	OH in 4(c): 0.0, 0.0, 0.1930, occ = 1/2
	H in 4(e): 0.0, 0.0, 0.0617, occ = 1/2

[a] occ stands for occupancy.

(21). Atomic positions of OHAp determined by Kay *et al.* (22) from X-ray diffraction data were used (Table 1).

RESULTS AND DISCUSSION

Chemical analysis of Ca and P reveals that the synthesized OHAp sample is stoichiometric (i.e., molar ratio Ca/P = 1.667). All X-ray diffraction maxima can be indexed on the basis of the OHAp unit cell (23). Infrared spectrum analysis performed on this sample shows the typical absorption bands of hydroxyapatite. Two characteristic absorption bands at 1090–1050 cm^{-1} correspond to the antisymmetric stretching vibration mode of the phosphate group. A single absorption band at 960 cm^{-1} can be assigned to the symmetric vibration mode, and the two bands at 600 and 570 cm^{-1} correspond to the bending mode of the phosphate group. Finally, two adsorption bands at 3570 cm^{-1} (stretching mode) and 630 cm^{-1} (bending mode) can be assigned to the OH group (24, 25).

Electron microscopy observations have been performed on the synthesized stoichiometric OHAp sample $Ca_{10}(PO_4)_6(OH)_2$. As long as the JEOL 2000FX microscope has a structure resolution limit of 0.31 nm, there is not enough resolution to solve atom clusters in the OHAp structure (19); therefore, the lattice image along the [0001] zone axis (Fig. 1) is not an atomic structure image. The projection sixfold hexagonal symmetry with a clear absence of mirror planes parallel to the c-axis is apparently conserved in some areas (see the area marked A in Fig. 1) and is reflected in the corresponding microdiffraction pattern (left inset).

Simulated images (Fig. 2) show a quite satisfactory match with the structure image at $\Delta f = 150$ nm (part A in Fig. 1) and for $\tau = 5.5$ nm crystal thickness. However, the lattice image in part B does not fit the calculated image, probably because of crystal tilt; the corresponding microdiffraction pattern in part B of the crystal shows some deviation from the perfect sixfold hexagonal symmetry, which is possibly related to the crystal tilt of area B with respect to area A. Therefore, the anomalous behavior of the lattice image in part B may be due to local elastic-bending distortion of the specimen (26). However, the possible existence of beam tilt with respect to the crystal cannot be excluded, as it also distorts the image at higher thickness (27). Areas of white contrast in Fig. 1 (marked C) are possibly due to thickness and density variations related to local Ca/P stoichiometry (11, 12).

The possible presence and detection of the OHAp monoclinic form by converging beam electron diffraction (CBED) have recently been discussed (17). Both the monoclinic and hexagonal types of OHAp are very similar (Table 2). The distribution of hexagonal and twin-related monoclinic domains by means of 120° rotation about the c-axis has been reported (18, 20). However, it is still not clear if there is any possible transformation from the hexagonal to the monoclinic form as a consequence of beam irradiation.

The formation of CaO and (α-TCP) during TEM irradiation damage observations has also been reported (7, 8, 10, 16). The decomposition of OHAp at high temperatures can be described as

$$2\ Ca_5(PO_4)_2(OH) \rightarrow 3\ Ca_3(PO_4)_2 + CaO + H_2O.$$

When OHAp is heated at 1050°C it converts partially to β-TCP, as observed in the X-ray diffraction pattern (28). On the other hand, the formation of α-TCP when OHAp decomposes at high temperatures during TEM observation could be explained in terms of chemical reactions occurring under conditions far from equilibrium which may also depend on incident beam energy and/or crystal orientation (29).

Specimen irradiation damage may be due to direct displacements (knock-on collisions), radiolysis effects due to the ionization of the specimen elements, or rise in temperature due to energy loss by the electrons along their trajectory in the irradiated material (30–35). However, it is widely accepted that damage due to a single mechanism rarely occurs.

Figure 3a shows the zero-order Laue zone (ZOLZ) microdiffraction pattern of an OHAp crystal along the [0001] orientation. The sixfold symmetry can be observed. In addition, the first-order Laue zone (FOLZ) is also visible although with very weak intensity. Using the formula

$$H = 2/\lambda\ (R/CL)^2,$$

where H stands for the spacing between ZOLZ and FOLZ (in nm), R stands for the FOLZ radii (in nm), and CL is the camera constant in (mm × nm), the repeat distance along the c-axis can be approximately calculated (36), giving a value of $H = 0.7$ nm, which is very close to that for the OHAp c-axis ($c = 0.688$ nm).

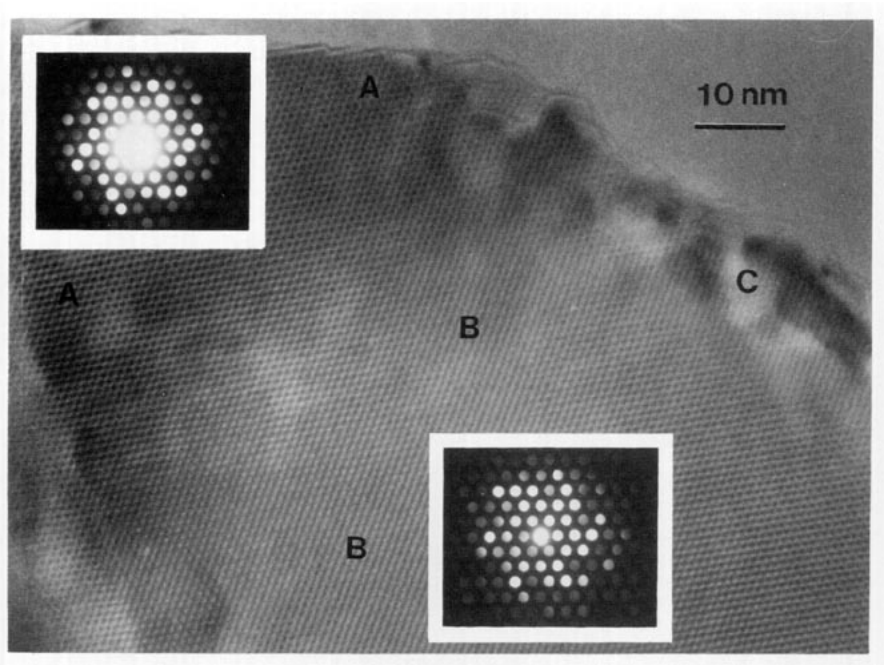

FIG. 1. Image of an OHAp crystal along the [0001] direction. Left inset: microdiffraction pattern taken at the left part (A) of the crystal. Right inset: the microdiffraction pattern taken at the lower part (B) of the crystal.

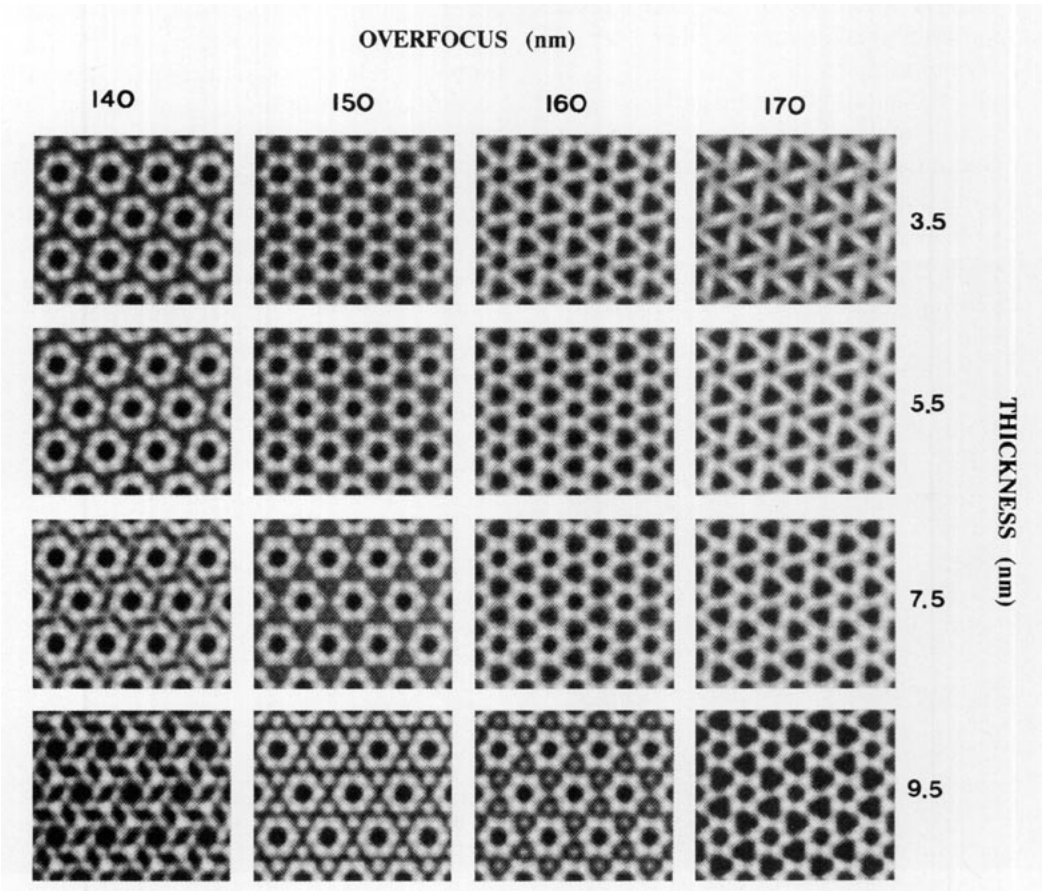

FIG. 2. Through-focus series of computed simulated images of the OHAp structure along the [0001] zone. On each image 4 × 4 unit cells are shown (C_s = 2.3 mm, C_c = 2.2 mm).

TABLE 2
Crystal Structures of Some Compounds Often Found with OHAp

Compound	Symmetry	Lattice parameters
Hydroxyapatite ($Ca_{10}(PO_4)_6(OH)_2$)	Monoclinic ($P2_1/b$)	a = 0.963 nm $b = 2a$, c = 0.688 nm $\gamma = 120°$
α-Tricalcium phosphate (α-$Ca_3(PO_4)_2$)	Orthorhombic	a = 1.522 nm b = 2.071 nm c = 0.9109 nm
β-Tricalcium phosphate (β-$Ca_3(PO_4)_2$)	Rhombohedral ($R3m$)	$a = b$ = 1.042 nm c = 3.74 nm
Calcium oxide (CaO)	Cubic ($Fm3m$)	$a = b = c$ = 0.481 nm
Octacalcium phosphate ($Ca_8H_2(PO_4)_6 \cdot 15H_2O$)	Triclinic (P_1)	a = 0.954 nm, $\alpha = 92.5°$ b = 1.90 nm, $\beta = 90.0°$ c = 0.686 nm, $\gamma = 79.9°$
Brushite ($CaHPO_4 \cdot 12H_2O$)	Monoclinic	a = 0.636 nm, $\beta = 118.5°$ b = 1.519 nm c = 0.581 nm

After 5 min of irradiation, the sixfold symmetry is still maintained and the FOLZ still appears with the same repeat distance along the c-axis, as observed in the microdiffraction pattern shown in Fig. 3b. The above results are found to be reproducible over several OHAp crystals along the [0001] orientation.

On the other hand, the microdiffraction pattern aligned along $[2\bar{1}\bar{1}0]$ zone axis shows a 2-mm projection symmetry with only weak intensity visible within the $(000l)$ (l = odd) reflections (Fig. 4a). After few minutes of irradiation under the electron beam, a FOLZ ring appears with a corresponding repeat distance along $[2\bar{1}\bar{1}0]$ of 0.99 nm (Fig. 4b). The same crystal was then tilted to the $[1\bar{1}00]$ orientation; from the FOLZ ring, the corresponding repeat distance is found to be 1.67 nm (Fig. 4c).

Those repeat distances of 1.67 and 0.99 nm deduced from corresponding FOLZ rings along $[1\bar{1}00]$ and $[2\bar{1}\bar{1}0]$ orientations, respectively, are observed over several irradiated OHAp crystals. According to our observations, such FOLZ rings are not detected before beam heating (see Figs. 4a and 4d).

The presence of the monoclinic form of OHAp (with $b = 2a$) is not detected in our X-ray diffraction pattern. On the other hand, according to the above observations, the sixfold symmetry along the [0001] orientation is apparently conserved even after beam heating. Although the OHAp $P21/b$ monoclinic phase and the hexagonal ($P63/m$) give identical ZOLZ patterns along this zone axis (17), the existence of 1.67 and 0.99 nm repeat distances along $[1\bar{1}00]$ and $[2\bar{1}\bar{1}0]$, respectively, indicates that some crystal structure transformation takes place under beam irradiation.

On the other hand, the weak intensity observed, in general, in the $(000l)$ (l = odd) reflections of beam irradiated crystals (not allowed by the $P63/m$ space group) is probably related to such a space group transformation.

Although the observed spacings at 1.67 and 0.99 nm could be described on the basis of a monoclinic cell (with $c_{hex} = c_{monoc}$ and $a_{monoc} = 2b_{hex}$, $d_{010} = 1.64$ nm, $d_{1\bar{1}0} =$

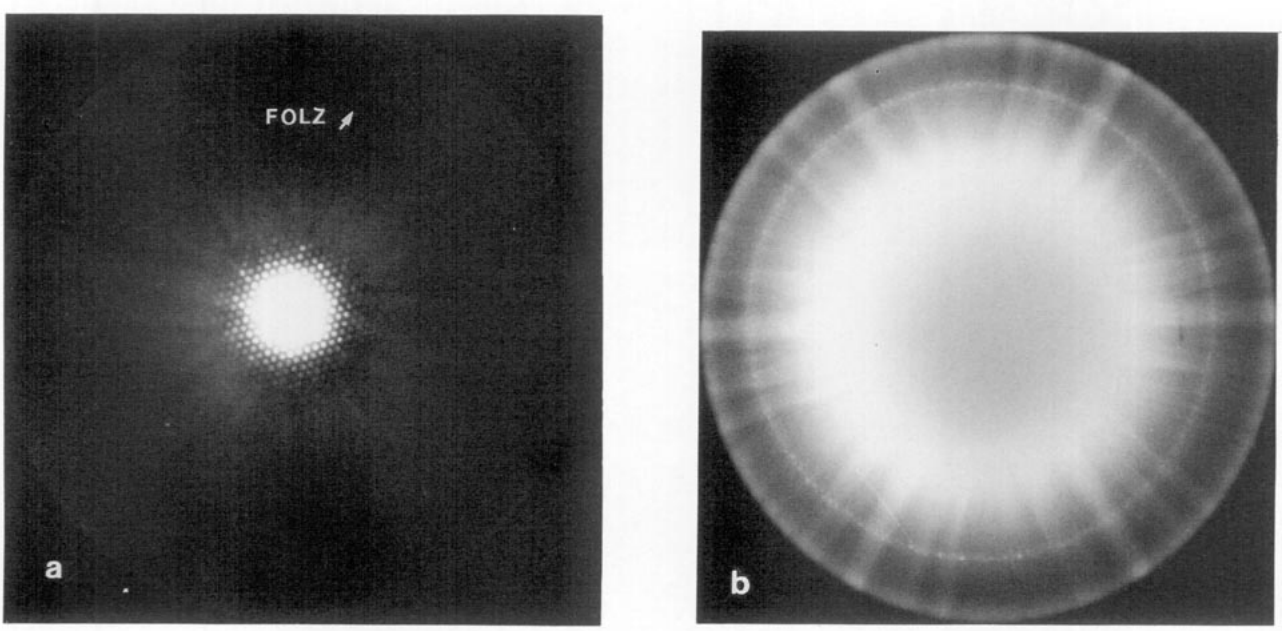

FIG. 3. (a) The microdiffraction pattern of OHAp oriented along the [0001] zone axis; (b) the same pattern as shown in (a) after 5 min of irradiation; the sixfold symmetry is still maintained. The pattern is overexposed in order to better observe the appearance of sixfold symmetry.

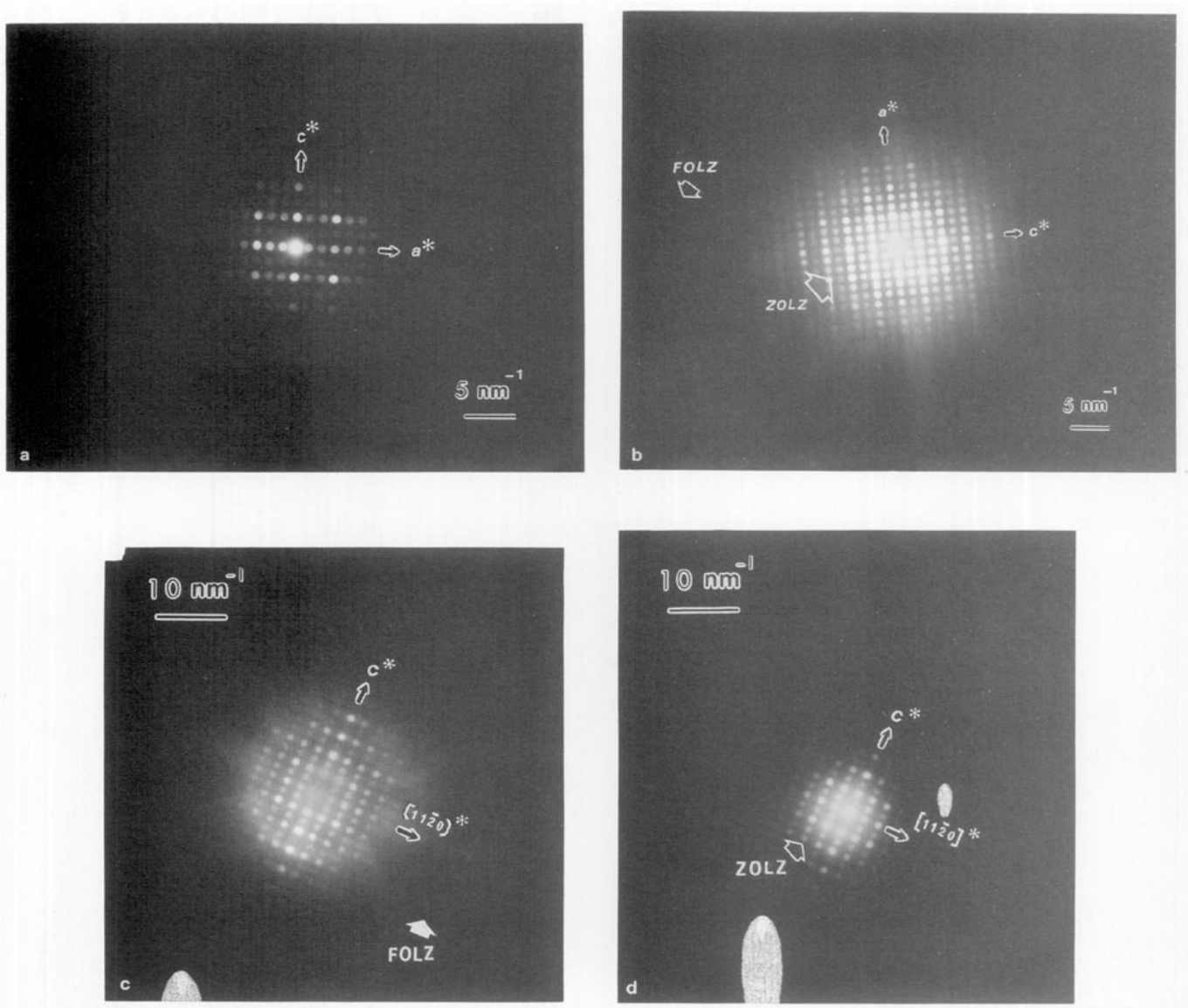

FIG. 4. (a) MDP of OHAp viewed along the [2$\bar{1}\bar{1}$0] zone axis, before irradiation; 2 mm symmetry is observed; (b) MDP of the same crystal along the [2$\bar{1}\bar{1}$0] zone axis after 5 min of irradiation; a FOLZ ring appears; (c) MDP of the same crystal (already irradiated) tilted to [1$\bar{1}$00] orientation; a FOLZ ring is apparent; (d) MDP of OHAp crystal along [1$\bar{1}$00] before irradiation.

0.95 nm), the presence of other phases previously reported (see Table 2) with large crystal parameters cannot be excluded.

In order to obtain further information on the nature of the observed structural changes under irradiation, the sensitive Moiré fringe method has been used. Moiré fringe patterns have proven to be not only an excellent tool for the detection of very small local crystal spacing variations (undetectable in the image or diffraction pattern), but also to enhance the effects of rotations, defects, and strain fields (37–41). Such an example is given in Figs. 5a, 5b, and 5c, where a clear evolution of the Moiré pattern as a function of the irradiation time is observed along [2$\bar{1}\bar{1}$0].

The corresponding optical diffraction taken from the Moiré fringe area (Fig. 6) clearly shows matrix OHAp spots and spots at d = 0.335 nm (marked by arrows) which are slightly misaligned from the exact parallel position to the (0001) matrix row. These extra spots could be attributed to the presence of a second phase. Now, as long as the irradiation experiments along the [0001] zone axis indicate that the compound remains hexagonal (or even monoclinic), because the sixfold axis is maintained and the presence of other phases (Table 2) is less probable

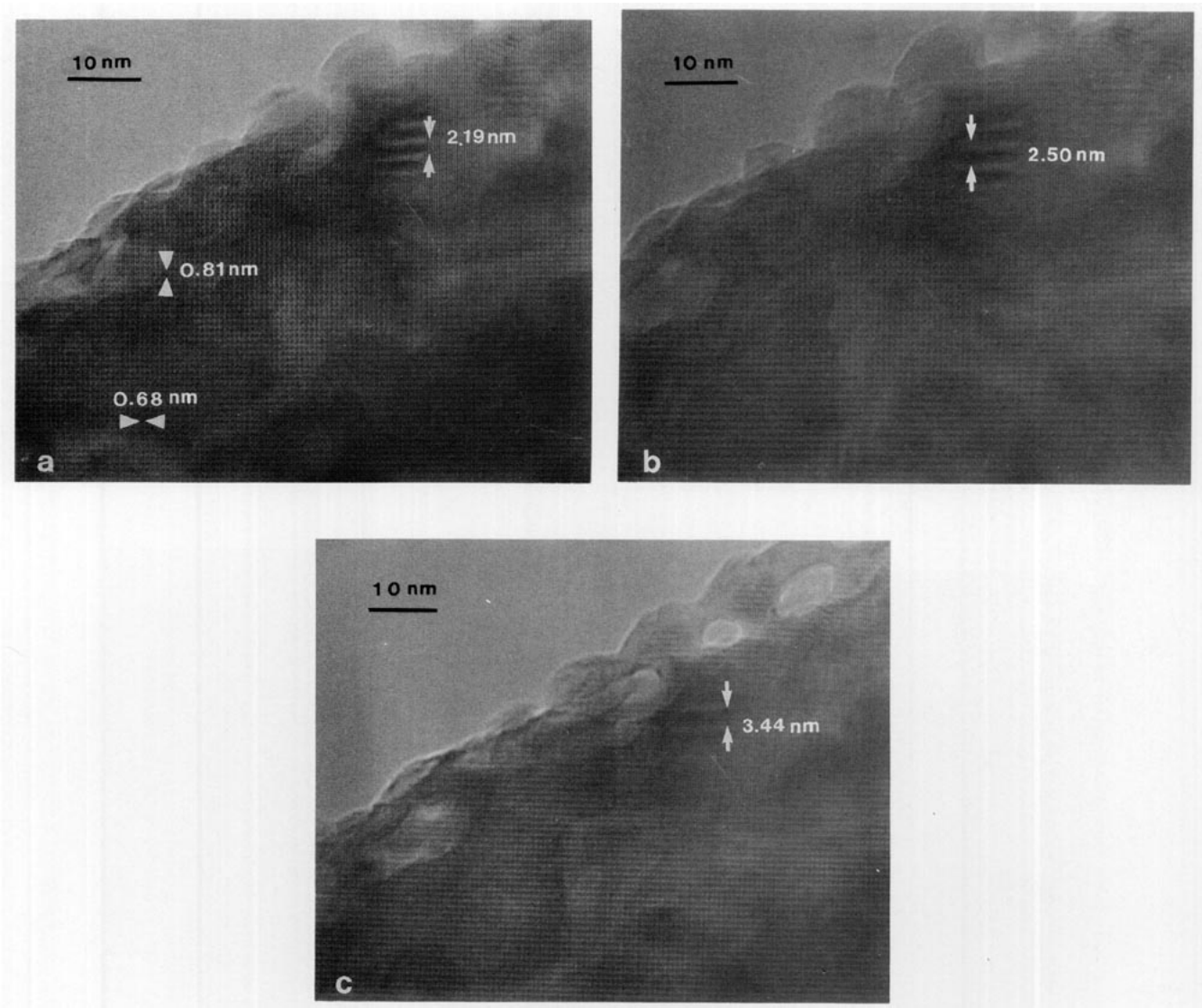

FIG. 5. OHAp crystal aligned along the [2$\bar{1}$10] zone axis. Increasing irradiation time (t = 0, 1, and 2 min in panels (a)–(c), respectively) gives rise to the change of the Moiré fringe period.

since they are undetectable in our electron diffraction patterns, it could be supposed that the extra spots at d = 0.335 nm correspond to the d_{0002} spacing of a second OHAp'.

Moiré fringe patterns are generated from the interference between lattice planes, namely, d_{0002}(OHAp) = 0.335 nm and d_{0002}(OHAp') = 0.344 nm. The direction of the fringes is perpendicular to the line joining the pair of the $(0002)_{OHAp}$ and $(0002)_{OHAp'}$ spots. The observed Moiré fringe patterns may be analyzed by means of the well-known formula (41)

$$D = \frac{d_{OHAp} d_{OHAp'}}{(d^2_{OHAp} + d^2_{OHAp'} - 2d_{OHAp} d_{OHAp'} \cos \phi)\, 1/2}, \quad [1]$$

where ϕ is the rotation angle between those misoriented planes and D stands for the Moiré fringe period. The analysis of the evolution D and ϕ with irradiation leads to the values gathered in Table 3. In the table, the observed values of Moiré D spacings (Fig. 5) are compared to those values calculated with the d_{0002}(OHAp) and d_{0002}(OHAp') lattice parameters and Eq. [1]. Rotation angle values ϕ can be observed directly on the optical diffractograms of Fig. 6; the evolution of D spacings with beam heating is related to the small changes of angle ϕ observed in Figs. 6a and 6b.

From the above observations it can be concluded that the change in period D in the Moiré fringe pattern could be due to a local rotation of a probable second OHAp'

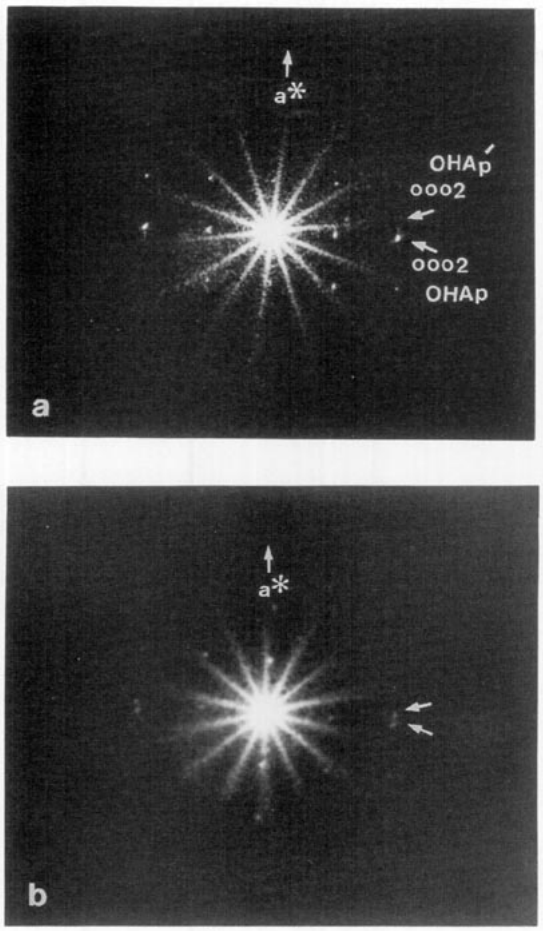

FIG. 6. (a) Optical diffractogram taken from the Moiré region of Fig. 5a. (b) Optical diffractogram taken from the Moiré region of Fig. 5c.

phase in relation to the OHAp matrix. On the other hand, direct comparison of the optical diffractograms shown in Figs. 6a and 6b indicates that $d_{10\bar{1}0}$ and d_{0002} spacings of the OHAp matrix are not altered by beam heating.

The disorder created in the OHAp structure by beam irradiation has been extensively studied (7–17). It is possible that the observed very small local crystal rotations, which are undetectable in the electron diffraction patterns, are related to stoichiometric changes and order–disorder transformations (e.g., changes in a space group from $P63/m$ to monoclinic).

TABLE 3
Evolution of Moiré Fringes with Irradiation

Irradiation time	D_{obs}(nm)	D_{calc}(nm)	ϕ_{obs}(°)
t = 0 min	2.19	2.46	8.0(5)
t = 2 min	2.50	2.83	7.0(5)
t = 4 min	3.44	3.95	5.0(5)

Another example of the usefulness of the Moiré fringe patterns in detecting small crystal variations can be observed in Figs. 7a, 7b, and 7c where a series of structural images along $[2\bar{1}\bar{1}0]$, at different time intervals of irradiation, is shown. A Moiré fringe pattern may be formed as a consequence of beam damage, as long as end products following OHAp decomposition are formed at the surface and/or the bulk of the OHAp structure.

The optical diffraction pattern taken from the Moiré pattern area (Fig. 8a) shows the presence of slightly misoriented spots (marked with arrows) from the exact parallel position in relation to the matrix $(10\bar{1}0)$ OHAp row. This spot, corresponding to d = 0.278 nm spacing, could be attributed to the intense $(21\bar{3}1)$ OHAp reflection ($d_{21\bar{3}1}$ = 0.281 nm). According to previous work (7), image simulation experiments demonstrate that the most probable beam-induced (at 300 kV) end product in OHAp crystals is in fact CaO; therefore, this spot could also be attributed to the $(111)_{CaO}$ reflection. Nevertheless, as long as electron diffraction patterns along [0001] indicate that the sixfold symmetry is maintained after irradiation, we assume that this extra spot probably belongs to the $d_{21\bar{3}1}$ spacing of another OHAp″ surface-formed microcrystal.

In this case, since the misalignment angle of the two lattice plane spacings (namely, $d_{30\bar{3}0}$(OHAp) = 0.272 nm and $d_{21\bar{3}1}$(OHAp″) = 0.278 nm) is small (ϕ = 6.5°), Moiré fringe patterns may be generated from the interference between them.

According to Eq. [1], the calculated period of Moiré fringes is D_{calc} = 2.34 nm, in good agreement with the experimentally determined one, D_{exp} = 2.39 nm, directly measured on the optical diffractogram and on the photograph plate.

If we suppose now that the new phase is indeed CaO and the observed spacing d = 0.278(5) nm corresponds to the $(111)_{CaO}$ distance (0.277 nm) then, applying Eq. [1], the calculated Moiré period D is found to be D_{calc} = 2.40 nm; as can be observed, the CaO presence could also be compatible with the experimentally observed Moiré D_{exp} spacing.

The fringe pattern shown in Fig. 7a and 7b satisfies the standard criteria for Moiré fringe regarding their spacing and orientation, and it is perpendicular to the line joining the pair of optical diffraction spots which combine to form the Moiré pattern.

In this case, the crystal formed at the surface, which probably shows the OHAp structure, is oriented slightly off the exact two-beam condition for the assumed $(21\bar{3}1)$ OHAp reflection, because of crystal tilt. Moiré fringes are more sensitive to tilts than the high-resolution pattern is, and this can be used to detect tilts in the HREM image (42).

In the series of pictures taken at different irradiation

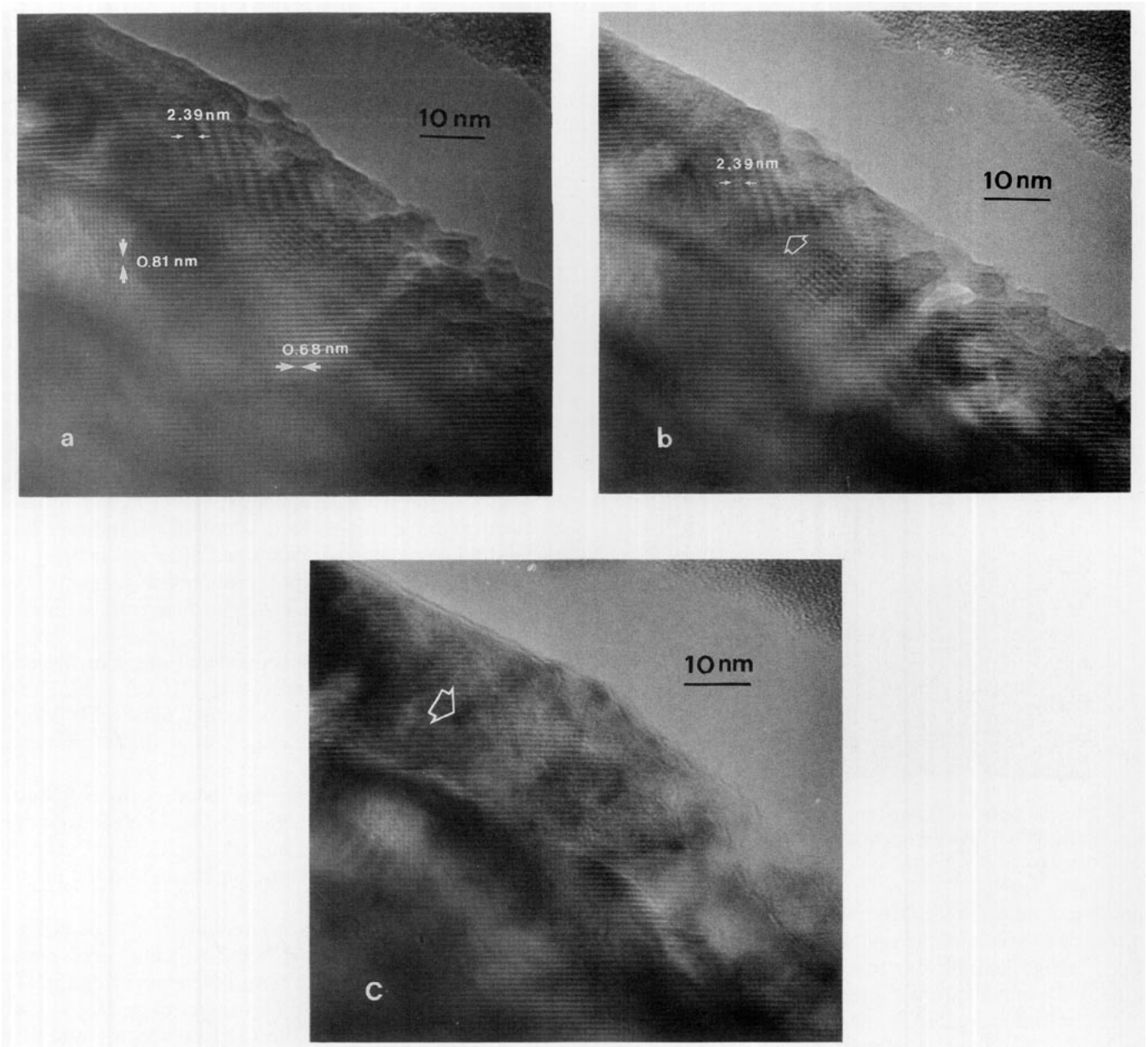

FIG. 7. OHAp crystal aligned along the [$2\bar{1}\bar{1}0$] zone axis. Panels (a)–(c) have been observed at increasing irradiation times (t = 0, 3, and 6 min, respectively). In (c), the Moiré fringe pattern previously observed (see arrow) has disappeared.

times (Figs. 7a–7c), the evolution of Moiré fringes is clearly observed. Their spacing and their orientation in relation to the substrate have not changed, although they are slightly displaced as a whole (see Fig. 7b). Finally, their contrast almost disappears with time (Fig. 7c).

Such a behavior could be explained from the results of the dynamical theory of Moiré pattern formation (43, 44). In fact, the direction of the fringes and their spacing are not influenced by a variation of thickness of the two overlapped crystals or by a slight variation of their orientation in relation to the electron beam. Nevertheless, according to the dynamical diffraction theory, the details of the Moiré fringe pattern will be continuously modified during tilting. Although the direction and the spacing of the Moiré fringes remain unaltered, the fringes are displaced and the contrast between dark and bright fringes and their intensities varies. For thin crystals, a well-defined Moiré pattern should disappear rather slowly during tilting and should not reappear, or, at least, should reappear only vaguely (43).

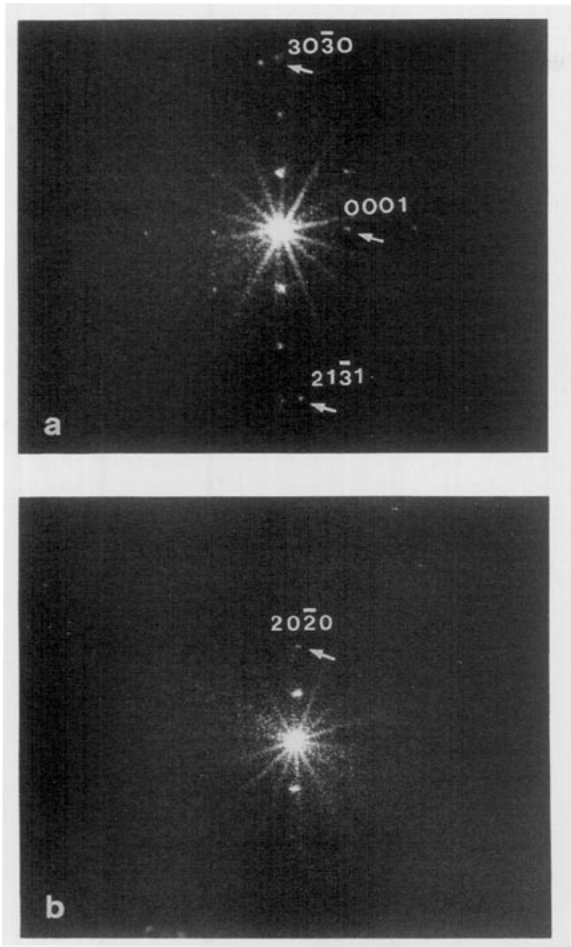

FIG. 8. (a) Optical diffractogram taken from the Moiré region of Figs. 3a and 3b. (b) Optical diffractogram of the arrowed area of Fig. 3c. The crystal has been tilted toward the [0001] diffraction spot.

Therefore, we can conclude that our experimental results from the observed Moiré patterns agree with the previously theoretical predictions; in addition, crystal tilt is also evidenced from the optical diffraction pattern (Fig. 8b).

CONCLUSIONS

Beam-induced transformations in OHAp-type structures leading to the formation of CaO and α-$Ca_3(PO_4)_2$ are strongly dependent on the initial stoichiometry of the irradiated OHAp structure and/or the energy of the incidence beam. It seems probable that electron beam irradiation induces stoichiometry changes. On the other hand, observed d spacings from corresponding FOLZ rings in electron diffraction patterns of OHAp stoichiometric irradiated samples may be related to a possible hexagonal to monoclinic phase transformation (e.g., $P63/m$ to monoclinic with $b = 2a$).

The Moiré fringe method has proved to be a very useful tool, since it is possible to detect local phase transformations inside the OHAp structure, which are otherwise undetectable in the electron diffraction patterns. Order–disorder transformations in the OHAp structure seem to be related to very small local lattice rotations, which, in turn, are detectable by the changing of the period of Moiré fringe patterns under beam heating. Moreover, the behavior of Moiré fringes with continuous tilting of the crystal is consistent with the dynamical diffraction theory, proving the sensibility of this method in the detection of very small crystal variations.

ACKNOWLEDGMENTS

Financial support from the Comisión Interministerial de Ciencia y Tecnología (CICYT, Spain) through research Projects MAT 91-0331 and MAT 93-0207 is acknowledged. We also thank J. L. Baldonedo and R. Ropero for technical assistance.

REFERENCES

1. M. Jorcha, J. F. Kay, K. I. Gumaer, R. H. Doremus, and K. P. Drobeck, *J. Bioeng.* **1,** 79 (1977).
2. J. L. Katz and R. A. Harper *in* "Encyclopedia of Materials Science and Engineering" (M. B. Berver, Ed), Vol. I, p. 474. Pergamon Press, New York, 1986.
3. W. F. Neumann and M. W. Neumann, *in* "Chemical Dynamics at Bone Mineral," p. 39. Univ. of Chicago Press, Chicago, 1958.
4. D. R. Simpson, *Clin. Orthop.* **86,** 260 (1972).
5. R. A. Young, *J. Dent. Res.* (*suppl.*) **53,** 193 (1974).
6. C. C. Basset, R. J. Pawluk, and R. Becker, *Nature* **204,** 652 (1964).
7. E. F. Bres, J. L. Hutchison, B. Senger, J. C. Voegel and R. M. Frank, *Ultramicroscopy* **35,** 305 (1991).
8. J. l. Huaxia and P. M. Marquis, *J. Mater. Sci. Lett.* **10,** 132 (1991).
9. J. D. B. Featherstone, D. G. A. Nelson, and J. D. McLean, *Caries Res.* **15,** 278 (1981).
10. D. G. Nelson and J. D. Featherstone, *Calcif. Tissue Int.* **34,** 569 (1982).
11. T. Aoba, J. Takahashi, T. Yagi, M. Okazaki, and Y. Moriwaki, *J. Dent. Res.* **57,** 708 (1978).
12. T. Aoba, J. Takahashi, T. Yagi, Y. Doi, M. Okazaki, and Y. Moriwaki, *J. Dent. Res.* **60,** 954 (1981).
13. E. F. Bres, J. C. Voegel, and R. M. Frank, *J. Microsc.* **160,** 183 (1990).
14. D. G. A. Nelson, G. J. Wood, J. C. Barry, and J. D. B. Featherstone, *Ultramicroscopy* **19,** 253 (1986).
15. D. G. A. Nelson and J. C. Barry, *Anat. Rec.* **224,** 265 (1989).
16. B. Senger, E. F. Bres, J. L. Hutchinson, J. C. Voegel, and R. M. Frank, *Philos. Mag.* (*Part*) *A* **65**(3), 665 (1992).
17. E. F. Bres, D. Cherns, and R. Vincent, *Acta Crystallogr. Sect. B* **49,** 56 (1993).
18. P. E. Mackie, J. C. Elliot, and R. A. Young, *Acta Crystallogr. Sect. B* **28,** 1850 (1972).
19. E. F. Bres, J. C. Barry, and J. L. Hutchison, *J. Ultrastruct. Res.* **99,** 261 (1985).
20. J. C. Elliott, P. E. Mackie, and R. A. Young, *Science* **180,** 1055 (1973).
21. R. Kilaas, *in* "Proceedings 45th Annual Meeting of EMSA" (G. W. Bailey, Ed.), p. 66. 1987.
22. M. I. Kay, R. A. Young, and A. S. Possner, *Nature*, **204,** 1050 (1964).

23. Powder X-ray Data File, ASTM 9-432.
24. E. E. Berry, *J. Inorg. Nucl. Chem.* **29,** 317 (1967).
25. S. R. Radin and P. Ducheyne, *J. Mater. Sci.* **3,** 33 (1992).
26. M. I. Buckett, J. Strane, D. E. Luzzi, J. P. Zhang, B. W. Wessels, and L. D. Marks, *Ultramicroscopy* **29,** 217 (1985).
27. D. J. Smith, W. O. Saxton, M. A. O'Keefe, G. J. Wood and W. M. Stobbs, *Ultramicroscopy* **11,** 263 (1983).
28. Powder X-ray Data File, 9-169.
29. V. S. Nagarajan and K. J. Rao, *J. Mater. Chem.* **3,** 43 (1993).
30. L. Reimer, *in* "Physics of Image Formation and Microanalysis" Chap. 10. Springer-Verlag, Berlin, 1984.
31. J. C. K. Spence, "Experimental High Resolution Electron Microscopy," p. 212. Oxford Univ. Press, Oxford, 1988.
32. M. L. Knotek, P. J. Feibelman, *Phys. Rev. Lett.* **40,** 964 (1978).
33. D. Menzel and R. Gomer, *J. Chem. Phys.* **41,** 3311 (1964).
34. P. A. Redhead, *Can. J. Phys.* **42,** 886 (1964).
35. N. Itoh and T. Nakayama, *Phys. Lett. A* **92,** 471 (1982).
36. R. Ayer, *J. Electron Microsc. Tech.* **13,** 16 (1989).
37. K. Hashimoto and R. Uyeda, *Acta Crystallogr.* **10,** 143 (1957).
38. L. A. Bursill, J. L. Hutchison, N. Sumida, and A. R. Lang, *Nature* **192,** 518 (1981).
39. C. S. Pande, *Solid State Commun.* **37,** 753 (1981).
40. C. D. Hetherington, *Mater. Res. Soc. Symp. Proc.* **183,** 123 (1990).
41. P. B. Hirsch, A. Howie, R. B. Nicholson, D. W. Pashley, and M. J. Whelan, "Electron Microscopy of Thin Crystals," p. 343. Butterworths, London, 1965.
42. J. P. Faure and G. Nihoul, *Philos. Mag.* (*Part*) *A* **61,** 245 (1990).
43. R. Gevers, *Philos. Mag.* **VII,** 1681 (1962).
44. B. Pardo, C. Pariset, and D. Renard, *Phys. Status Solidi A,* 283 (1981).